Aerosol direct, indirect, semidirect, and surface albedo effects from sector contributions based on the IPCC AR5 emissions for preindustrial and present-day conditions

Susanne E. Bauer[1,2] and Surabi Menon[3]

Received 1 September 2011; revised 9 November 2011; accepted 16 November 2011; published 14 January 2012.

[1] The anthropogenic increase in aerosol concentrations since preindustrial times and its net cooling effect on the atmosphere is thought to mask some of the greenhouse gas-induced warming. Although the overall effect of aerosols on solar radiation and clouds is most certainly negative, some individual forcing agents and feedbacks have positive forcing effects. Recent studies have tried to identify some of those positive forcing agents and their individual emission sectors, with the hope that mitigation policies could be developed to target those emitters. Understanding the net effect of multisource emitting sectors and the involved cloud feedbacks is very challenging, and this paper will clarify forcing and feedback effects by separating direct, indirect, semidirect and surface albedo effects due to aerosols. To this end, we apply the Goddard Institute for Space Studies climate model including detailed aerosol microphysics to examine aerosol impacts on climate by isolating single emission sector contributions as given by the Coupled Model Intercomparison Project Phase 5 (CMIP5) emission data sets developed for Intergovernmental Panel on Climate Change (IPCC) AR5. For the modeled past 150 years, using the climate model and emissions from preindustrial times to present-day, the total global annual mean aerosol radiative forcing is -0.6 W/m^2, with the largest contribution from the direct effect (-0.5 W/m^2). Aerosol-induced changes on cloud cover often depends on cloud type and geographical region. The indirect (includes only the cloud albedo effect with -0.17 W/m^2) and semidirect effects (-0.10 W/m^2) can be isolated on a regional scale, and they often have opposing forcing effects, leading to overall small forcing effects on a global scale. Although the surface albedo effects from aerosols are small (0.016 W/m^2), triggered feedbacks on top of the atmosphere (TOA) radiative forcing can be 10 times larger. Our results point out that each emission sector has varying impacts by geographical region. For example, the single sector most responsible for a net positive radiative forcing is the transportation sector in the United States, agricultural burning and transportation in Europe, and the domestic emission sector in Asia. These sectors are attractive mitigation targets.

Citation: Bauer, S. E., and S. Menon (2012), Aerosol direct, indirect, semidirect, and surface albedo effects from sector contributions based on the IPCC AR5 emissions for preindustrial and present-day conditions, *J. Geophys. Res.*, *117*, D01206, doi:10.1029/2011JD016816.

1. Introduction

[2] Climate forcing by greenhouse gases is known accurately as discussed in the *Intergovernmental Panel on Climate Change* (*IPCC*) [2001, 2007] reports, but some of the greenhouse gas warming is masked by the presence of other climate forcing agents, such as ozone, land use or cryosphere changes, solar irradiance, or aerosols, that have positive and negative feedbacks on the climate system. Aerosol climate forcing is complex because aerosols both reflect solar radiation to space and absorb solar radiation. In addition, atmospheric aerosols alter cloud cover and cloud properties. Historically, aerosols have been studied by each single chemical component (sulfate, nitrate, black carbon, organic carbon, dust and sea salt), and more recently, aerosols from particular source sectors on radiative forcings (RF) have been studied by economic activity. *Koch et al.* [2007] separated present-day forcing effects of industry, residential, power, transport, biomass burning, and natural emissions according to the Emission Database for Global Atmospheric Research (EDGAR) emission data set and concluded that large negative RF comes mostly from power and industry

[1]NASA Goddard Institute for Space Studies, New York, New York, USA.
[2]Earth Institute, Columbia University, New York, New York, USA.
[3]Lawrence Berkeley National Laboratory, Berkeley, California, USA.

0148-0227/12/2011JD016816

sector. Sectors with net positive forcing are residential and transportation due to their considerable emissions of black carbon. An extension of this study by *Unger et al.* [2008], where IPCC A1B emissions for the year 2030 were used to estimate direct radiative forcings from specific emission sectors for aerosols and ozone, finds results fairly similar to those of *Koch et al.* [2007].

[3] These prior studies included the interplay of absorbing and reflecting aerosols but did not consider any detailed aerosol microphysics. Aerosol microphysical processes such as nucleation, condensation, and coagulation determine the mixing state and size distribution of aerosols, which are important characteristics, e.g., to calculate aerosol optical properties and cloud activation. Especially when discussing the effects of black carbon (BC) aerosols, it is important to consider aerosol coatings that enhance absorption. Black carbon-rich emission sectors such as the transportation sector have become the focus of short-term mitigation studies. Although the overall effect of aerosols is cooling, the question has been raised if the aerosol cooling effect on climate could be made stronger by reducing the absorbing aerosol components from the aerosol mix.

[4] Recent studies, all using climate models with aerosol microphysics and aerosol-cloud effects, examined the effects of soot on clouds and solar absorption and concluded fairly different results. *Jacobson* [2010] (hereafter referred to as J10) suggested that fossil fuel and biofuel soot may be considered as the second leading cause of global warming after CO_2 and that controlling their emission sources may be the fastest way to reduce Arctic ice loss and global warming. *Chen at al.* [2010] (hereafter referred to as C10) estimated that net changes in top of the atmosphere (TOA) cloud radiative forcing are +0.13 (fossil fuel mitigation) and +0.31 W/m^2 (fossil fuels, biofuels, and biomass burning) but only discussed an estimated indirect effect, while J10 discussed the response of climate to complete BC removal. *Bauer et al.* [2010, p. 7439] (hereafter referred to as B10) found that "Black carbon mitigation scenarios generally show reduced radiative fluxes when sources with a large proportion of BC, such as diesel, are reduced; however reducing sources with a larger OC component, such as biofuels warms the climate." and a study by *Koch et al.* [2011a, p. 1051] (hereafter referred to as K11) including several global models performing identical emission reduction scenarios concludes that "The nonlinearities resulting from the competition of opposing effects on the cloud condensation nuclei (CCN) population make it difficult to extrapolate from idealized experiments to likely impacts of realistic potential emission changes." The results of these studies appear to be different, but it has to be taken into account that J10 and C10 tested the effect of BC emission per se and B10 and K11 more feasible and therefore much less drastic, emission reduction scenarios. However, all these studies agree that the direct effect of BC-rich fuels is leading to a positive forcing and that the indirect effect is either negative (C10, K11) or a small positive. The disagreement among J10, C10, B10, and K11 was introduced by semidirect effects that were absent in C10 and completely dominating the results in J10 and of importance in B10 and K11. Note that J10 also included rather strong absorption effects of BC due to processes like BC inclusion in clouds and BC interstitially between cloud particles, effects that are not necessarily included in all other studies. However, none of these studies quantified or further examined the impact of semidirect effects.

[5] A review paper [*Koch and Del Genio*, 2010] on semidirect effects of absorbing aerosols such as BC or dust summarized the multiple effects absorbing aerosols can have on clouds by absorbing incoming solar radiation, perturbing the temperature structure of the atmosphere, and influencing cloud cover. The review paper found that semidirect effects depend on several factors, including the altitude of the aerosols relative to the cloud and the cloud type. Most global model studies indicate a regional variation in the cloud response but generally increased cloud cover over oceans and some land regions, with net increased low-level and/or reduced upper level cloud cover. The result is a net negative semidirect effect feedback from the cloud response to absorbing aerosols. In this study we investigate the semidirect effect due to aerosol changes by emission sector, a combination of reduction of absorbing and scattering aerosols. Scattering aerosols themselves can induce semidirect effects, triggered by less solar radiation that is reaching the Earth surface, similar to solar dimming effects.

[6] We describe the experimental setup (section 2), discuss simulations including climate change and the role of aerosols in that context (section 3) and the forcing and feedbacks of the single emission sectors (section 4), and conclude the paper with a general discussion (section 5).

2. Experimental Setup

[7] The Goddard Institute for Space Studies (GISS) General Circulation Model (GCM) "modelE" [*Hansen et al.*, 2005; *Schmidt et al.*, 2006] coupled to the aerosol microphysics and chemistry model MATRIX (Multiconfiguration Aerosol Tracker of mixing state) [*Bauer et al.*, 2008] is used in this study, and a brief description is provided in Appendix A. The setup of the aerosol microphysical scheme MATRIX is identical concerning aerosol microphysics and aerosol radiation coupling as described by *Bauer et al.* [2010]. Regarding aerosol-cloud coupling, only the first indirect effect (cloud albedo effect) is taken into account. The second indirect effect (aerosol influence on autoconversion and precipitation) is not included in this work. Further improvements are the increased model resolution to 2° latitude by 2.5° longitude and 40 vertical hybrid sigma layers from the surface to 0.1 hPa, updated GCM physics as developed for the IPCC AR5 simulations (see Appendix A), and the use of the Coupled Model Intercomparison Project Phase 5 (CMIP5) historical emissions for the period (1850–2000) by *Lamarque et al.* [2010].

[8] This inventory is used in chemistry model simulations needed by climate models for the CMIP5 in support of the Intergovernmental Panel on Climate Change (IPCC) Fifth Assessment Report (AR5) (to be published in 2014). Estimates for the year 2000 inventory represent a combination of existing regional and global inventories to capture the best information available at this point; 40 regions and 12 sectors are used to combine the various sources. The historical reconstruction of each emitted compound, for each region and sector, is forced to agree with our 2000 estimate, ensuring continuity between past and 2000 emissions. Previous work conducted with the GISS model [e.g., *Koch*

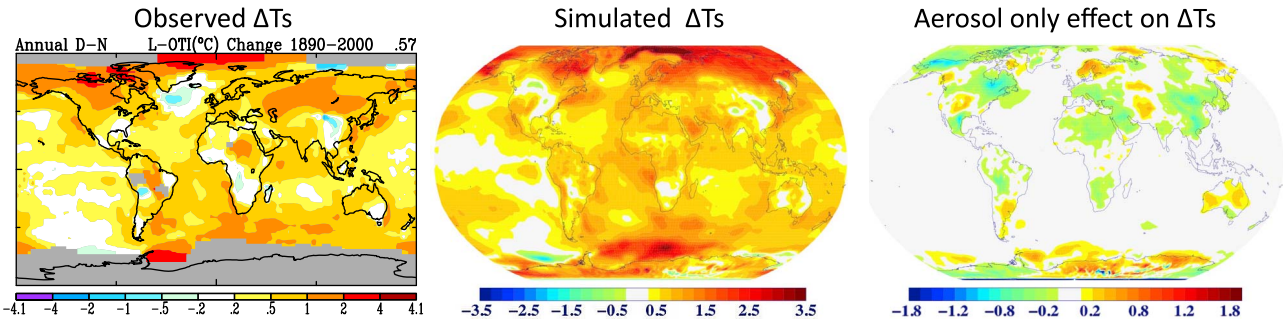

Figure 1. (left) Surface air temperature (K) differences between 2000 and 1890 in the GISS temperature analysis, (middle) simulated surface air temperature change between 2000 and 1850 (PD-PI) and (right) aerosol contribution only (PD-PIa).

et al., 2001b; *Bauer et al.*, 2010; *Unger et al.*, 2010] used emission information from data sets that were the basis for the CMIP5 inventory such as the EDGAR [*Bond et al.*, 2004] and the Global Fire Emissions Database (GFED). The main differences between those data sets are in the preindustrial concentrations of anthropogenic carbonaceous emissions and biomass burning, which are much higher in the CMIP5 inventory than in the previous used estimates. In this study, natural emissions are kept identical in all experiments to ensure clean diagnosis of the CMIP5 emission changes. The following natural emissions were included: volcano (24.3 Tg SO_2), vegetation (16.8 Tg OM), oceans (31.4 Tg DMS, 9.8 Tg NH_3, 4400 Tg sea salt), and desert dust (1600 Tg silt and clay).

[9] Sea surface temperatures are prescribed as boundary conditions. The model is not coupled to the gas-phase ozone chemistry scheme. Off-line fields of oxidants and nitric acid concentrations are provided as input fields from a previous coupled chemistry–aerosol simulation. Off-line ozone and greenhouse gas fields are provided for forcing calculation in the model radiation scheme. Model simulations are integrated for 11 years, and 10 year mean conditions are discussed in this paper.

[10] We discuss direct (Fd), indirect (Fi), semidirect (Fs), and surface albedo (Fa) effects. Distinguishing these four radiative forcing mechanisms requires additional model simulations using net (shortwave + longwave) instantaneous forcings (Rf) at the top of the atmosphere. The anthropogenic aerosol forcing is diagnosed from the difference between the fluxes from the present-day year 2000 (PD) and a preindustrial year 1850 (PI) simulations. PI simulations are calculated for aerosol emission changes only (PIa), using PD atmospheric (GHG, etc.) and sea surface temperature (SST) conditions, and a full PI simulation, where PI emission, atmospheric and SST conditions are used.

Radiative flux changes due to all forcings

$$\mathrm{Ft\_clima} = \mathrm{Rf(PI)} - \mathrm{Rf(RD)}$$

Radiative flux changes due to aerosols only

$$\mathrm{Ft} = \mathrm{Rf(PIa)} - \mathrm{Rf(RD)}$$

Direct radiative forcings (Fd) are calculated during the simulations, with double calls to the radiation including and excluding aerosols in the longwave and shortwave radiative transfer calculations. We use instantaneous forcings at the tropopause. Adjusted forcing, allowing stratospheric temperatures to respond, would be nearly identical for aerosols.

[11] Indirect effects are calculated by taking the difference between runs that include and exclude ($\mathrm{Rf_{noIE}}$) the coupling between NC and CDNC (described by *Menon et al.* [2010] and in Appendix A); hence, it includes the microphysical coupling between aerosol concentrations and clouds but only for the first indirect effect (cloud albedo effect).

$$\mathrm{Fi} = [\mathrm{Rf(PIa)} - \mathrm{Rf_{noIE}(PIa)}] - [\mathrm{RF(PD)} - \mathrm{Rf_{noIE}(PD)}]$$

Semidirect forcing is diagnosed as a residual:

$$\mathrm{Fs} = \mathrm{Ft} - \mathrm{Fi} - \mathrm{Fd}$$

The surface albedo forcing (Fa) is calculated by taking the instantaneous difference between the TOA radiative flux with and without the snow BC albedo. Surface albedo forcing feedbacks are calculated from the radiation changes including and excluding ($\mathrm{Rf_{noSalb}}$) surface albedo changes due to aerosol deposition:

$$\mathrm{Fa} = [\mathrm{Rf(PIa)} - \mathrm{Rf_{noSalb}(PIa)}] - [\mathrm{RF(PD)} - \mathrm{Rf_{noSalb}(PD)}]$$

3. Present-Day to Preindustrial Forcing and Feedbacks

3.1. Climate Change

[12] In order to estimate climate change between atmospheric year 1850 and year 2000 conditions, we examine the differences between two model runs that were set up for those conditions, including atmospheric composition, greenhouse gas concentrations, sea surface temperature, and further atmospheric and planetary settings. During the 150 year time period the TOA radiation increased by 1.8 W/m^2, leading to a global-mean surface air temperature increase of 0.7°C.

[13] Surface air temperature trends are relatively well observed, (one example can be found at http://data.giss.nasa.gov/gistemp/), allowing us to compare our simulation to observations. Figure 1 shows the sea surface temperature change between 1890 and 2000 and the simulated temperature change between 1850 and 2000. The model was driven by observed sea surface temperatures; therefore, the temperature over land is our focus. The model simulates the temperature change and most regional features remarkably well and also captures the observed temperature decrease

Table 1. Global-Mean Model Diagnostics[a]

	PD	PD − PI	PD − PIa	PD_{noIE} − PIa_{noIE}
TOA energy balance (W/m^2)				
Net radiation	1.8	1.8 (154)	−0.6 (−18)	−0.5 (−15)
Absorbed SW	244.7	0.2 (0.1)	−0.6 (−0.3)	−0.5 (−0.2)
Net LW	−242.8	1.6 (−0.7)	−0.01 (0.01)	0.04 (−0.01)
Cloud SW	−50.2	−0.2 (0.4)	−0.7 (1.3)	−0.6 (1.2)
Cloud LW	16.7	0.0 (0.05)	0.02 (0.2)	0.02 (0.1)
Net aerosols	−3.4	−0.5 (14)	−0.4 (12)	−0.4 (11)
Surface energy balance (W/m^2)				
Net energy	1.81	1.8 (163)	−0.6 (−18)	−0.5 (−16)
Absorbed SW	173.7	−0.45 (−0.3)	−1.3 (−0.8)	−1.2 (−0.7)
Net LW	57.6	−1.6 (−3)	−0.1 (−0.2)	−0.2 (−0.4)
Sensible heat flux	−20.8	0.9 (−4)	0.3 (−1.5)	0.2 (−1.2)
Latent heat flux	91.5	0.2 (0.2)	−0.2 (−0.3)	−0.2 (−0.3)
Net Aerosols	−5.6	−1.1 (20)	−1.0 (18)	−0.9 (17)
Cloud cover (%)				
Total	56	−0.6 (−1)	0.01 (0.02)	0.1 (0.2)
High	29	0.7 (2.5)	0.001 (0)	0.004 (0.02)
Medium	15	−0.3 (−2.3)	−0.01 (−0.07)	−0.01 (−0.1)
Low	38	−1.2 (−2.9)	−0.01 (−0.02)	0.14 (0.4)
Cloud water (kg/m^2)				
Liquid	1.06	0.01 (1)	0 (−0.01)	0.002 (0.2)
Ice	0.09	0.001 (1.4)	0 (−0.3)	−0.0004 (−0.4)
CDNC (cm^3)				
Moist convective	95	0.3 (0.3)	−1 (−0.1)	-
Stratiform	87	14 (20)	15 (21)	-
Optical thickness				
AOD, aerosols	0.21	0.03 (15)	0.03 (15)	0.03 (14)
AAOD, absorbing	0.0073	0.002 (23)	0.002 (22)	0.002 (23)
COD, clouds	21.4	0.7 (3.5)	0.4 (1.8)	−0.02 (−0.08)
Aerosol load (Tg)				
Sulfates	1.46	0.8 (54)	0.8 (53)	0.7 (52)
Nitrates	0.17	0.1 (50)	0.06 (33)	0.07 (37)
Ammonia	0.16	0.08 (50)	0.08 (50)	0.08 (50)
Ammonium	0.34	0.2 (64)	0.2 (61)	0.2 (62)
Organic matter	0.7	0.15 (21)	0.15 (21)	0.11 (17)
Black carbon	0.07	0.04 (53)	0.04 (53)	0.03 (51)
Dust	24.7	1.3 (5)	1.3 (5)	0.3 (1)
Sea salt	7.46	0 (0)	0 (−0.5)	0 (0.4)
Aerosol water	87.6	2.1 (2)	2.5 (3)	2.8 (3)
Meteorology				
Surface air temperature (°C)	14.6	0.7 (5)	−0.01 (−0.01)	−0.01 (−0.01)
Relative humidity (%)	74.8	0.2 (0.3)	0.02 (0.02)	0.02 (0.04)
Precipitation (mm/d)	3.2	0.01 (0.2)	−0.01 (−0.3)	−0.01 (−0.3)

[a]Values are given for the present-day simulation (PD), absolute (and percentage) differences between PD and a preindustrial (PI), PD and PIa, and PD_{noIE} and PIa_{noIE}.

over China, southern Africa and Bolivia. Model and data disagree over western Canada. Surface cooling is linked to the influence of aerosols. Figure 1 (right) isolates the aerosol influence, through direct, indirect, semidirect and surface albedo effects, on surface temperature. In the Northern Hemisphere, anthropogenic aerosols have slowed (Europe), sometimes offset (United States), or even cooled (China) surface temperatures. Aerosol effects on surface temperature and humidity are responsible for the cooling that has occurred over wide regions in Southeast Asia, in parts of Africa, and in the Americas and correspond to the observed temperature trends. Such dimming and brightening effects are well observed by surface radiation measurements [*Wild et al.*, 2005]. In some places, e.g., central Eurasia, aerosols enhance surface warming, caused in our model simulation by the combined effects of strongly absorbing sulfate-coated black carbon particles and reduced cloudiness.

[14] Table 1 gives the budget for model runs including aerosol, SST, and greenhouse gas (GHG) changes (PD-PI), and aerosol changes only (PD-PIa). Due to climate change (PD-PI), total cloud cover decreases over the oceans, caused by a reduction in low clouds over the oceans, and cloud cover increases at high latitudes, caused by increased amounts of high level ice clouds. This results in a decreased cloud radiative forcing (CRF) over land and increased CRF over ocean, leading to a global mean decrease of -0.2 W/m^2. Hence, when considering the combined effect of aerosols impacts and global warming the overall effect of cloud changes results in a negative forcing globally, but with positive forcing contributions over the oceans. The tendency for high clouds to rise in such a way as to remain at nearly the same temperature as the climate warms seems to be a robust feature observed in several climate models [*Zelinka and Hartmann*, 2010].

[15] The TOA radiation has increased by 1.8 W/m^2 since 1850. Anthropogenic aerosols have Ft = -0.6 W/m^2. In sections 3.2–3.5 we diagnose mechanisms through which the different aerosol forcings (direct, indirect, semidirect, and surface albedo) contribute to the total forcing.

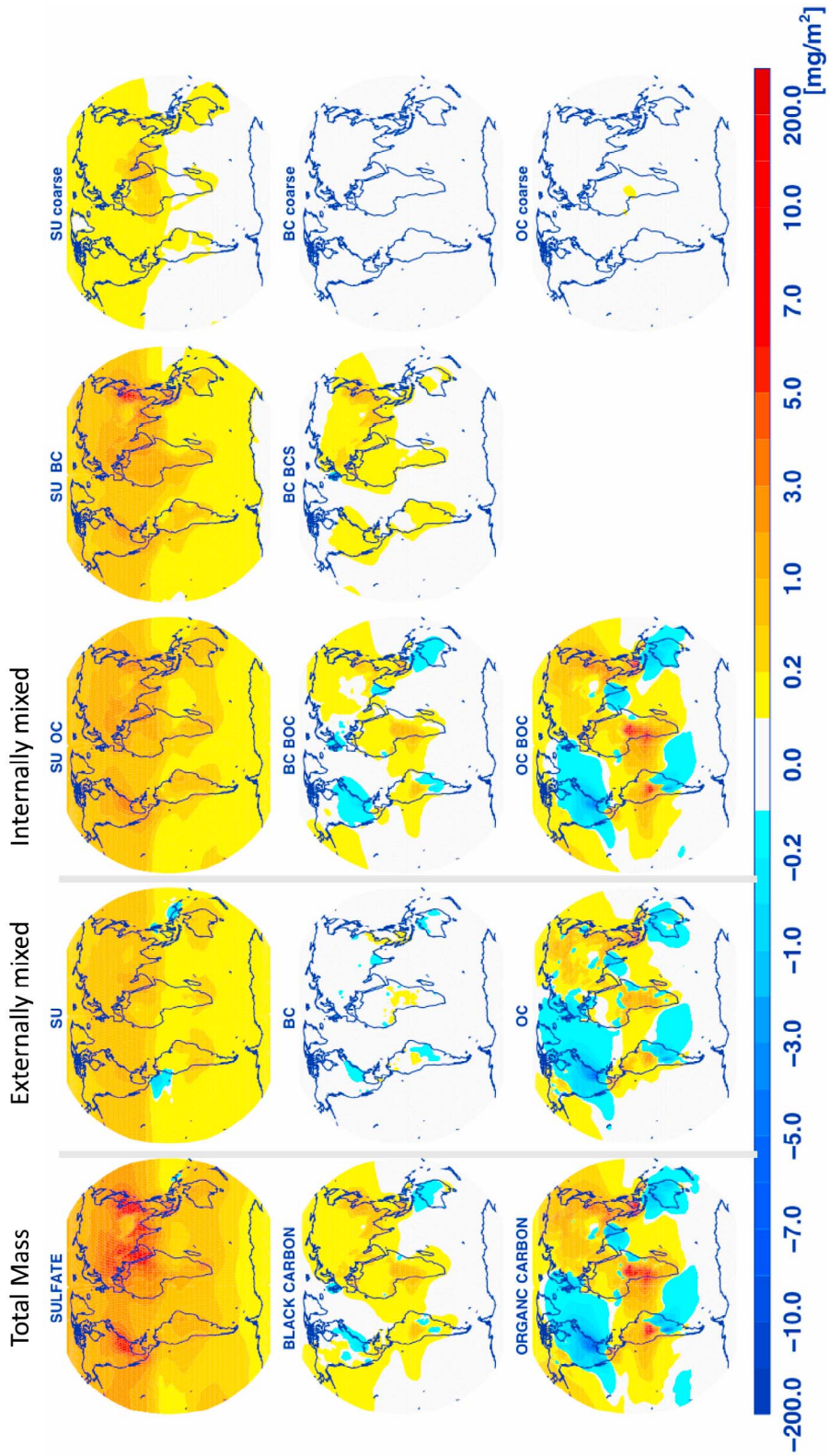

Figure 2. Aerosol load change between PIa and PD. From left to right, the total load of sulfate, black carbon, and organic carbon, their distributions into several mixing states, such as externally mixed, and the mixing ratio of SU, BC, or OC within the BOC (BC − OC mixtures), BCS (BC − sulfate mixtures) or coarse aerosol populations.

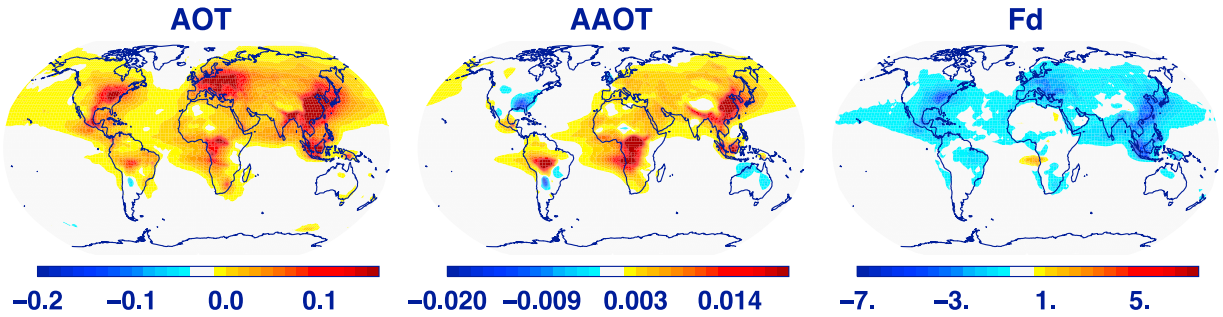

Figure 3. Aerosol optical thickness (AOT), absorption AOT (AAOT), and direct radiative Forcing (Fd) (W/m^2) as difference between PD and PIa.

3.2. Direct Aerosol Effects

[16] Aerosol loads of sulfates, nitrates, and black carbon material doubled in the past 150 years (Table 1). Organic matter emissions that were already high during preindustrial times due to forest clearings, domestic burning, and natural sources such as biomass burning and vegetation further increased globally by 20% due to enhanced biomass burning patterns in the Southern Hemisphere and increased emissions in Asia. Carbonaceous emissions decreased in North America during PD compared to the high emission during PI times when large amounts of biomass were burned for agricultural and domestic purposes. The impact on sulfate, BC, and OC loads and their mixing states are illustrated in Figure 2. Total sulfate loads increase everywhere as well as the sulfate mass in the different mixing states. The aerosol module MATRIX tracks 16 different mixing states, but to simplify this information, Figure 2 shows how much ammonium sulfate is externally mixed and how much sulfate is mixed primarily with OC, BC, or coarse aerosols. As already mentioned, biofuel and biomass BC and OC decrease in North America but due to a larger fraction of OC in biofuels and biomass OC decrease more strongly than BC which has enhanced fossil fuel sources at PD. BC/OC mixings decrease in the United States and some parts of Europe while BC mass in BC-sulfate mixtures increases. The change in BC mixing state has important implications on Fd. Aerosol optical thickness (Figure 3) increases globally by 15%, but aerosol absorption (AAOT) increases by 23%. Absorption decreases in the regions with decreased BC concentrations. Organic coatings enhance BC absorption by a factor of 2 to 3 [*Bauer et al.*, 2010].

[17] Aerosol direct radiative forcing Fd is −0.5 W/m^2 at the TOA and −1.1 W/m^2 at the surface, a 14% and 20% increase, caused by the differences in emissions between 1850 and 2000, respectively. *Bauer et al.* [2010], using the AR4 version of the model and AeroCom emissions, found that Fd was −0.11 W/m^2. However, the factor of 5 increase in Fd between these two versions is mainly caused by the differences in the emission inventories, especially for biomass burning.

[18] In the experiments where we neglect GHG and SST changes (PD − PIa) we see fairly similar changes in aerosol concentrations and forcings with the exception of ammonium nitrate, whose chemical production is more sensitive to temperature and humidity changes than other aerosol species.

3.3. Indirect Aerosol Effects

[19] Increased aerosol concentrations between PI and PD lead to a 20% increase in activated aerosol number concentrations, which on a global-mean basis translates into an increase of 15 cm^{-3}, with the largest increase of 400 (cm^{-3}) simulated over China. The aerosol populations that contribute most to activated particles are sulfates (+28%, numbers give percentage of number concentration change of activated particles by aerosol population), sea salts (−15%), organics (with coatings) (+22%), and BC-OC mixtures with coatings

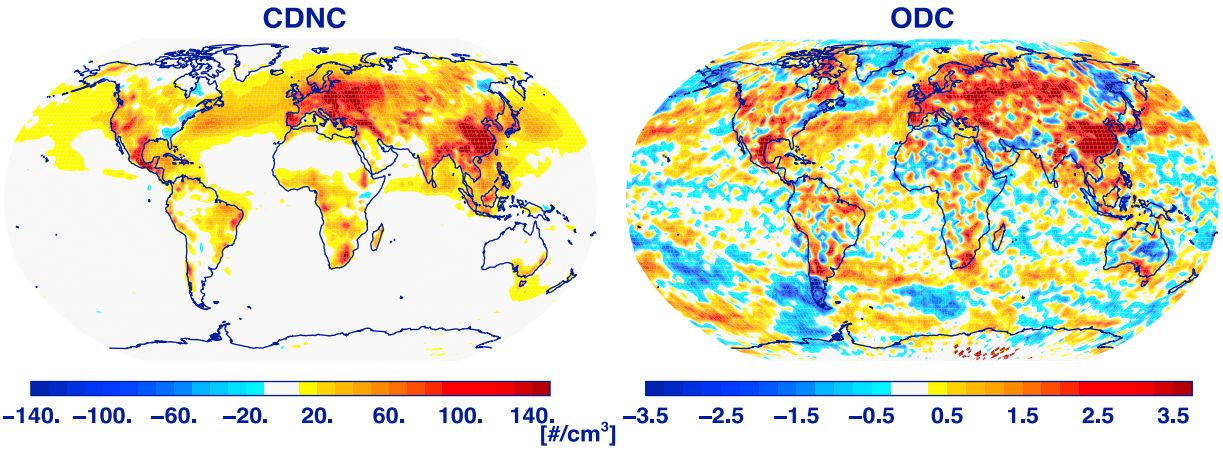

Figure 4. Cloud droplet number concentration (cm^{-3}) and cloud optical thickness change (PD-PIa).

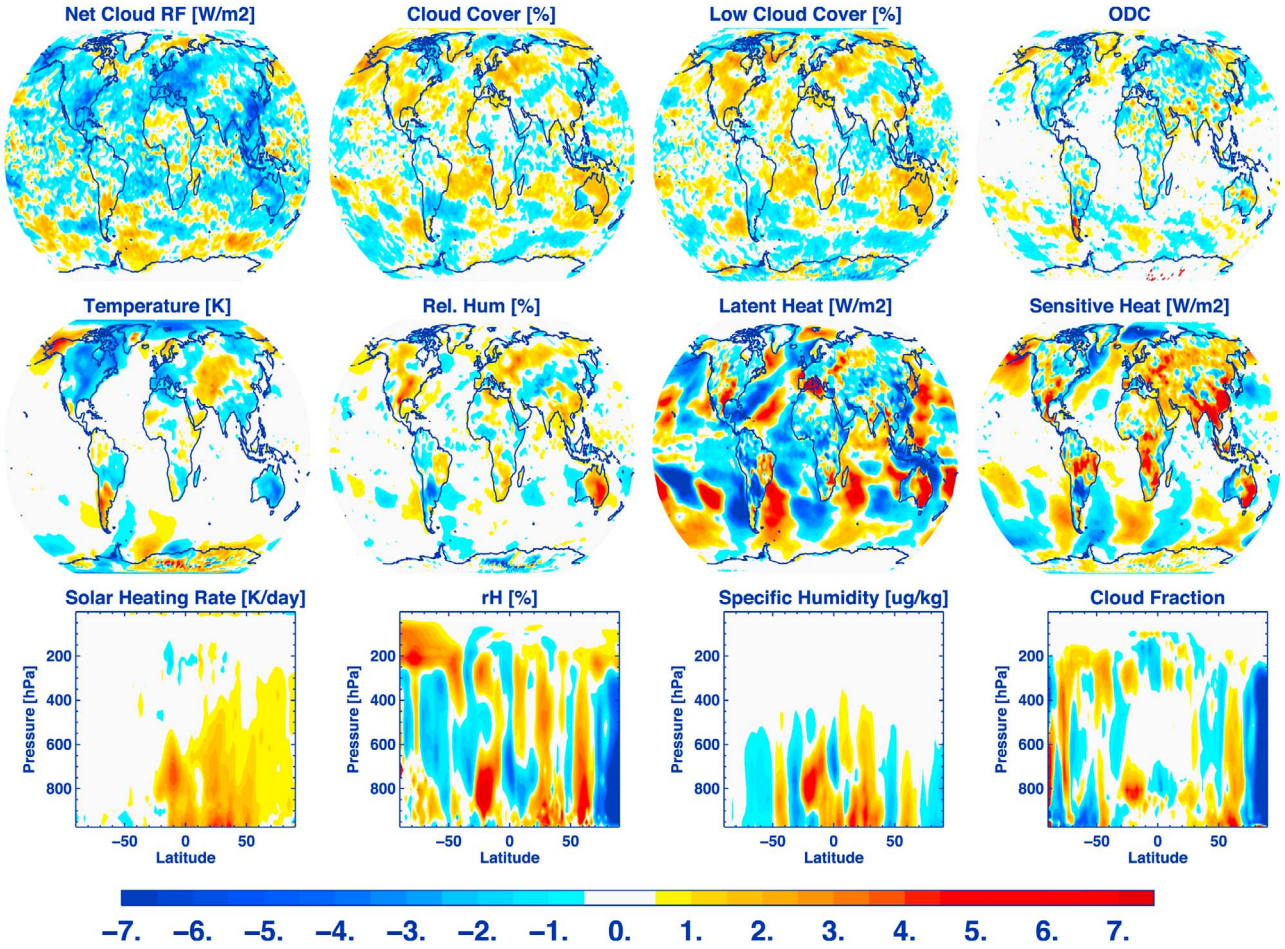

Figure 5. Differences (PD − PIa) in net cloud forcing, total cloud cover of optical thick clouds ($\tau > 1$), cloud cover of low clouds, cloud optical thickness, near-surface air temperature ($\times 10$), relative humidity, latent and sensitive heat flux. Zonal mean differences are shown for solar heating rates ($\times 100$), relative humidity, specific humidity, and cloud fraction.

(34%). The largest increase in activated number concentrations over China is mostly caused by sulfate- and nitrate-coated BC-OC particles, whereas their contributions in North America are decreased. Over Europe, sulfate and nitrate particles are most responsible for increase number concentrations. The portion of activated number concentrations that can grow into cloud droplets (CDNC) are shown in Figure 4. CDNC increase globally by 21% (note that this number is different from the activated particle number change due to further treatment of droplet microphysics), with more significant increases over Europe and China. The increased CDNC over the North Hemispheric Pacific and Atlantic are linked to increased concentrations in sulfate and sea salt mixtures in those regions. Enhanced CDNC increase cloud optical thickness (Figure 4) by 2%, leading to a Fi of -0.17 W/m^2.

3.4. Semidirect Aerosol Effects

[20] Semidirect effects are caused by several counteracting mechanisms as discussed in section 1 and summarized by *Koch and Del Genio* [2010], leading to increased and decreased cloudiness, depending on region, cloud type, and weather regime. The semidirect forcing Fs is calculated as a residual, and the diagnosed cloud changes (Figure 5) are the differences between PD and PIa of runs without microphysical aerosol-cloud interactions, or indirect effects.

[21] Cloud radiative forcing (calculated as double call to the radiation within the model, including and excluding clouds) is decreased during PD in the areas with high anthropogenic aerosol concentrations. This is caused by a reduction in optically thick clouds that are predominantly low clouds. Cloud optical thickness decreases over land, and it is interesting to note that when examining the combined climate effect, this might counterbalance the first indirect effect, which is characterized by increased cloud optical thickness (Figure 4). Surface temperature and relative humidity changes show colder and moister air over Europe, North America, India, and China and a stretch or warmer and dryer air between Europe and Asia. Sensitive heat flux changes are mostly positive over land, indicating warmer surfaces that are leading to upward heat releases into the atmosphere. The latent heat flux over land is mostly negative, indicating increased evaporation. Precipitation (not shown) does not change significantly over land areas but decreases in the intertropical convergence zone. The global mean change in precipitation is -0.3%. However, the largest

latent heat flux changes are simulated over the oceans, leading to the question of how fixed sea surface temperatures versus interactive ocean experiments would influence the results of this study (see section 5).

[22] While these results cannot directly be compared to other studies, it is interesting to note that *Randles and Ramaswamy* [2010] found a decrease in cloud amount and surface cooling and a slowing of the hydrological cycle over southern Africa, when scattering aerosols dominated absorbing aerosols in their study, with the Geophysical Fluid Dynamics Laboratory GCM that included the direct and semidirect aerosol effects for prescribed SSTs. This suggests that climate response to the semidirect effect would largely depend on simulated cloud response to aerosols and may be model specific.

[23] The heating caused by absorbing aerosols can be observed in the zonal mean distribution of the solar heating rate (Figure 5). Aerosols heat the surrounding air from 15°S throughout the entire Northern Hemisphere, but with peak zonal mean values of only about 0.1 K/d. In our model we do not observe cloud burn-off effects; we assume that these effects are rather small in our model, aided by the fact that we do not explicitly study the effect of absorbing aerosols but instead study the total effect of changing anthropogenic aerosols, which are absorbing and reflecting and thermodynamic effects driven by surface radiation changes that dominate in this model. This leads to fewer clouds in polluted regions and to a negative Fs of -0.1 W/m^2.

3.5. Surface Albedo

[24] Aerosol deposition on bright surfaces plays a special role because the bright surfaces can perturb the radiation balance of the Earth-atmosphere system in a number of ways. Direct aerosol forcing occurs through absorption or scattering. The added atmospheric heating will subsequently increase the downward longwave radiation to the surface, warming the surface. With the highly reflective surfaces typical in the Arctic, even a moderately absorbing aerosol can lead to a heating of the surface-atmosphere-aerosol column. Absorbing aerosols have an additional forcing mechanism when it is deposited on snow and ice surfaces [*Clarke and Noone*, 1985]. Such deposition enhances absorption of solar radiation at the surface, which can warm the lower atmosphere and induce snow and ice melting. Surface temperature responses are strongly linked to surface radiative forcings in the Arctic because the stable atmosphere of the region prevents rapid heat exchange with the upper troposphere. *Hansen and Nazarenko* [2004] have found that plausible estimates for the effect of soot on snow and ice albedos (1.5% in the Arctic and 3% in Northern Hemisphere land areas) yield a climate forcing of +0.3 W/m^2 in the Northern Hemisphere. The efficacy of this forcing is 2; that is, for a given forcing, it is twice as effective as CO_2 in altering global surface air temperature. Later studies estimate present-day global-mean radiative forcing from BC in snow to be +0.03 to +0.20 W/m^2 [*Hansen and Nazarenko*, 2004; *Jacobson*, 2004; *Flanner et al.*, 2007, 2009; *Koch et al.*, 2009].

[25] In this study the total BC ice and snow albedo forcing is 0.016 W/m^2 (16 mW/m^2), even smaller than the lower values of previous studies. Model evaluation [*Bauer et al.*, 2010] has shown that BC concentrations in high latitudes are most likely underestimated in the GISS-MATRIX model, and the increased resolution in this study has not changed that result. European BC concentrations usually agree well with observations, while BC concentrations in North America are already underestimated by a factor of 2 close to its sources. This indicates a low bias in North American BC emissions in the CMIP5 inventories. Also compared to profiles from aircraft data [*Bauer et al.*, 2010], we find BC to be well simulated in the tropics but underestimated in the polar region. Therefore, we interpret our estimates as biased low for possible impacts of trace gases on the Arctic.

[26] Even so, the BC ice and snow albedo forcing is 0.016 W/m^2. Performing a run with and without the impact of soot deposition on ice and snow, we see a difference in net TOA forcing of 0.11 W/m^2. This increase is caused by cloud feedbacks over the North Pole. North of 70°N, cloud cover typically ranges between 75% and completely overcast. Including BC ice and snow albedo forcing reduces cloud cover by 2%, leading to an additional positive TOA radiative forcing.

[27] The Arctic warms much faster than any other region on this planet. Observations (Figure 1) show that the global-mean surface temperature has increased by 1–4°C in the past 110 years. The Arctic and Antarctic are as well the only regions on Earth where aerosol effects lead to a net positive forcing over a large geographic area. When averaging surface air temperatures from 70°N to the North Pole, we see an increase of 2.1°C between 1850 and 2000. Isolating the aerosol-induced impact from this change, we see only a temperature increase of 0.1°C (see Figure 2). This rather small effect of aerosols on Arctic surface temperatures comes from the fact that aerosols lead to cooling of the polar region over the North American continent but to warming over Eurasia. Most cooling of Arctic surface temperature is associated with emissions from the energy, shipping, and industrial sector. Our simulated Arctic warming is due to emissions from grass and forest fires and to transportation, agricultural waste burning, and domestic sources (see Figure 9 in section 4).

[28] Here, we attempt to distinguish between forcings and feedbacks. Cloud changes are, by definition, feedbacks since we calculate the radiative change that occurs after the system has responded to a forcing pulse. Forcings are radiative disturbances that we apply to the system. However, we have demonstrated that for the direct radiative forcing we can use this approach but that surface albedo feedbacks differ quite substantially between induced radiative forcing and the resulting climate response. Since we diagnose a semidirect forcing as a residual forcing, we will exclude surface albedo effects from our sector forcing calculation so as not to misdiagnose surface albedo feedbacks with cloud feedbacks.

4. Sector Contributions to Forcings and Feedbacks

[29] The CMIP5 emission inventory provides 12 different sectors of emission activities. In this study we only report results of 10 different sector studies (Table 2) neglecting the waste and aviation sectors [*Unger*, 2011] because they have a very small impact when included as a single emission sector. The global emission fluxes for 1850 and 2000 are

Table 2. Emission Sectors

CMIP5 Sectors	Sensitivity Study
Energy production and distribution	Energy
Industry (combustion and noncombustion)	Industry
Land transport	Transportation
Maritime transport	Shipping
Aviation	-
Residential and commercial	Domestic (including solvents)
Solvents	
Agriculture	Agriculture
Agricultural waste burning on fields	AWB
Waste	-
Open vegetation fires in forests	Forest fires
Open vegetation fires in savanna and grassland	Grass fires

shown in Figure 6. First, we examine the direct forcing effects of each sector. The differences in TOA direct radiative forcings, Fd, between the base run and each run excluding the emissions of a single sector (sector minus base run) are presented in Figure 7.

[30] Globally, the energy sector is the largest emitter of SO_2 with relatively small contributions of other species. None of these emissions were present at PI, leading to a clear negative forcing of -0.13 W/m^2. Similar to the energy sector, maritime transport primarily emits SO_2 and results in a negative global forcing of -0.03 W/m^2. Agricultural emissions, in our inventory that only includes ammonia, are precursors for ammonium nitrate and ammonium sulfate, again leading to an increase of scattering aerosols and therefore have a negative forcing of -0.13 W/m^2 in the global mean. Energy and ship emissions show some positive forcing numbers in the Arctic caused by sulfate and nitrate coatings on absorbing aerosols.

[31] Industrial emissions contain large amounts of SO_2 and after the energy sector is the second largest emitter of SO_2. However, industrial processes are also a significant source of carbonaceous particles. Scattering and absorbing aerosols partly cancel each other; however, in areas like the United States and Europe the forcing is negative, and in China with high amounts of black carbon emitted from coal fire plants, the forcing is positive. The domestic emission sector is responsible for the highest anthropogenic emissions of black carbon and organic matter, especially in India, Southeast Asia, eastern Europe and Sub-Saharan Africa. Household cooking and wood burning release a mix of particles that instantly mix and form particles that mostly include black carbon, and lead to a positive forcing. Domestic emissions in western Europe and the United States contain a higher fraction of SO_2. Similar to the domestic sector, the transportation sector releases a mix of carbonaceous, SO_2, and NH_3 emissions, but this time releasing most of the black carbon in Europe and the United States, where it leads to a positive forcing. Agricultural waste-burning practices release relatively small amounts of emissions, compared to the other sectors, but are a significant contribution to aerosol forcing in the United States and Asia.

[32] Forest and grass fires are mostly of natural origin, but we include those two sources here in our quantification to understand their contributions to radiative forcing. Grass fires occur all over the world except in desert regions, but the

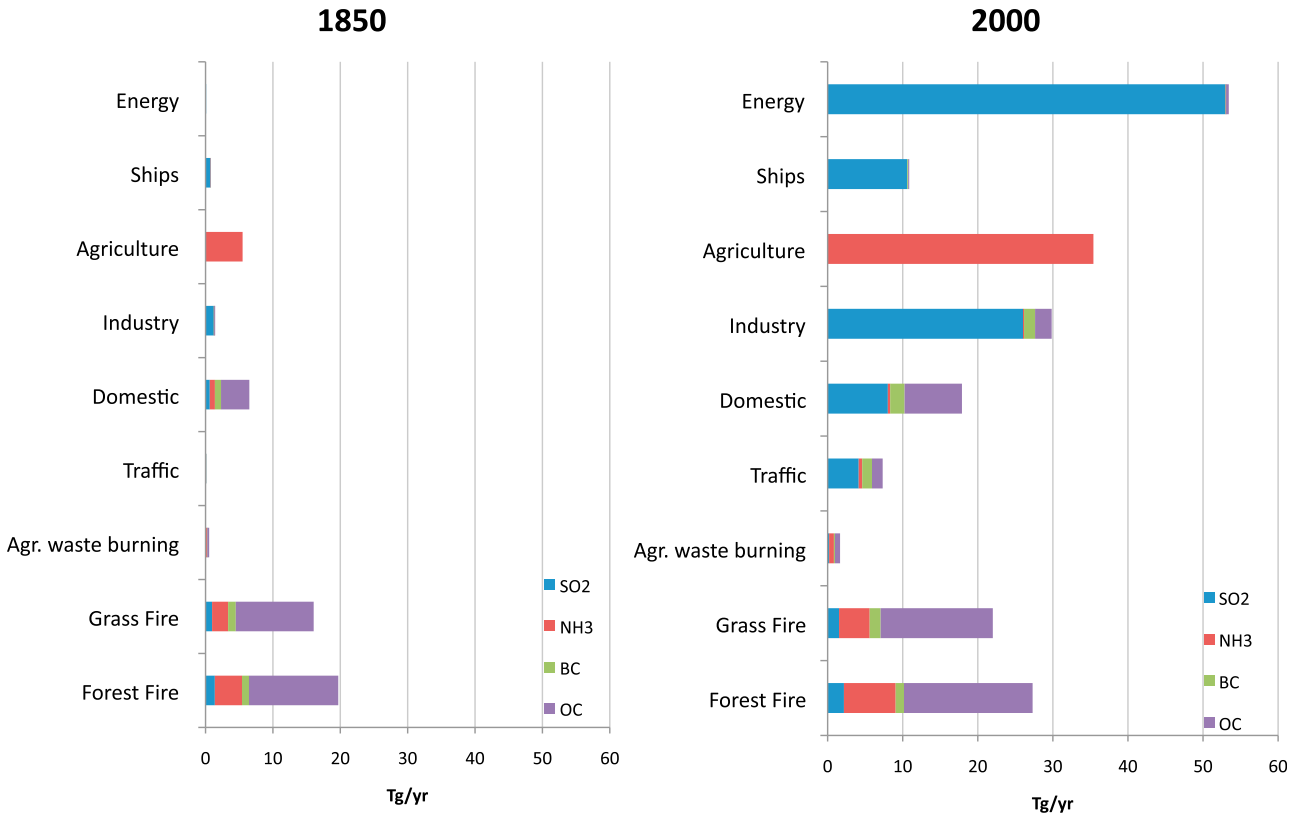

Figure 6. Annual mean emission fluxes (Tg/yr) by sector for years (left) 1850 and (right) 2000.

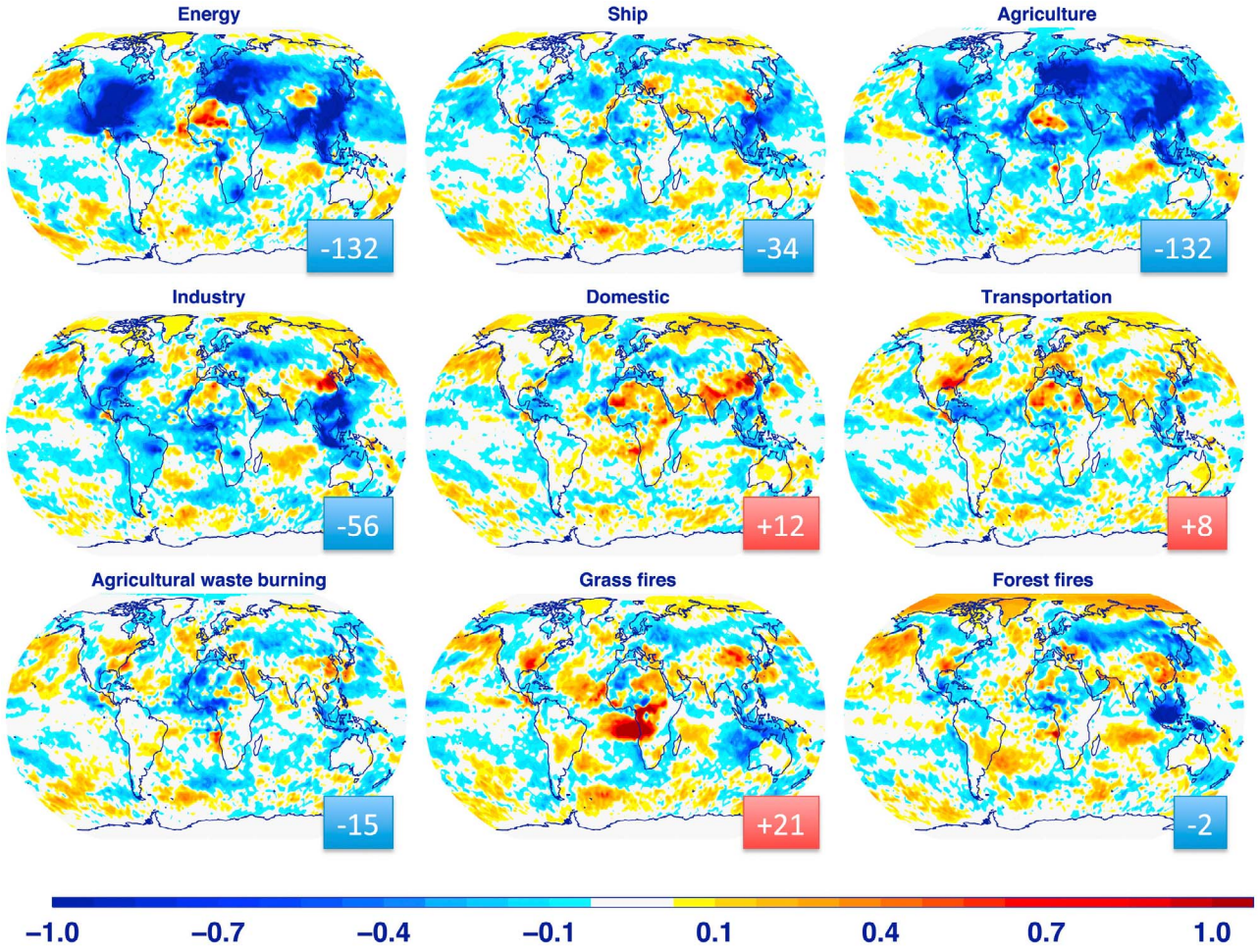

Figure 7. Differences in TOA radiative forcing (W/m^2) per emission sector between a base run and a sector experiment. The base run includes all emission sectors the sector run excludes one sector. The blue and red boxes give global-mean forcing numbers Fd (mW/m^2).

most intense grass fires develop in Africa, Brazil, and Australia, leading to a positive radiative forcing of 0.02 W/m^2. Forest fires on the other hand generally occur in high latitudes, South Africa, and Indonesia. Indonesian fires also burn peat, which results in particularly high emissions of ammonia that is responsible for the peak in negative forcing over that area. Owing to the fact that many forest fires are close to the Arctic Circle, they contribute most to the positive radiative forcing over the Arctic.

[33] To investigate aerosol-induced cloud changes, we first look at indirect effects. Figure 8 shows that the CDNC concentration changes by each sector experiment and gives its global percent change and Fi. Each sector provides a positive contribution to CDNC on a global basis, but regionally, CDNC concentrations can either increase or decrease and result in either a positive or a negative Fi. The results are presented in a way that shows the impact a sector has on CDNC distributions and Fi. For example, the energy sector is responsible for 12% of the PIa to PD change in CDNC and has an $Fi_{(energy)} = -0.12$ W/m^2.

[34] Only some sectors show noteworthy Fi changes. The energy and industry sector has a clear negative Fi signal, consistent with increased CDNC leading to optically thicker clouds, which reflect more radiation. But reducing the emissions of sectors rich with carbonaceous aerosols, e.g., transportation or grass or forest fires, can lead regionally to a reduction in CDNC concentrations. This phenomenon (as already discussed by *Bauer et al.* [2010]) is caused by the number concentration changes of the single mixing states. For example, a moderate reduction in BC emissions can lead to an increase in CDNC due to the fact that more sulfate material is either externally mixed or present within other mixtures, leading to higher number concentrations of cloud activating particles. Whether this leads eventually to increased or decreased CDNC depends on the amount (after a certain threshold, BC reducing leads to CDNC reduction) and the chemical composition (how much sulfate or OC is part of the emission) of the emission sector.

[35] The dissection of forcings by process, sector, and region is presented in Figure 9. Semidirect effects by sector on the global scale show very small forcing numbers because the regional effects can be either positive or negative which cancel each other out in the global mean. The uncertainty bars given in Figure 9 are calculated based on the year to year variability of the 10 year long simulations. Fd calculations are very robust, whereas the cloud-related

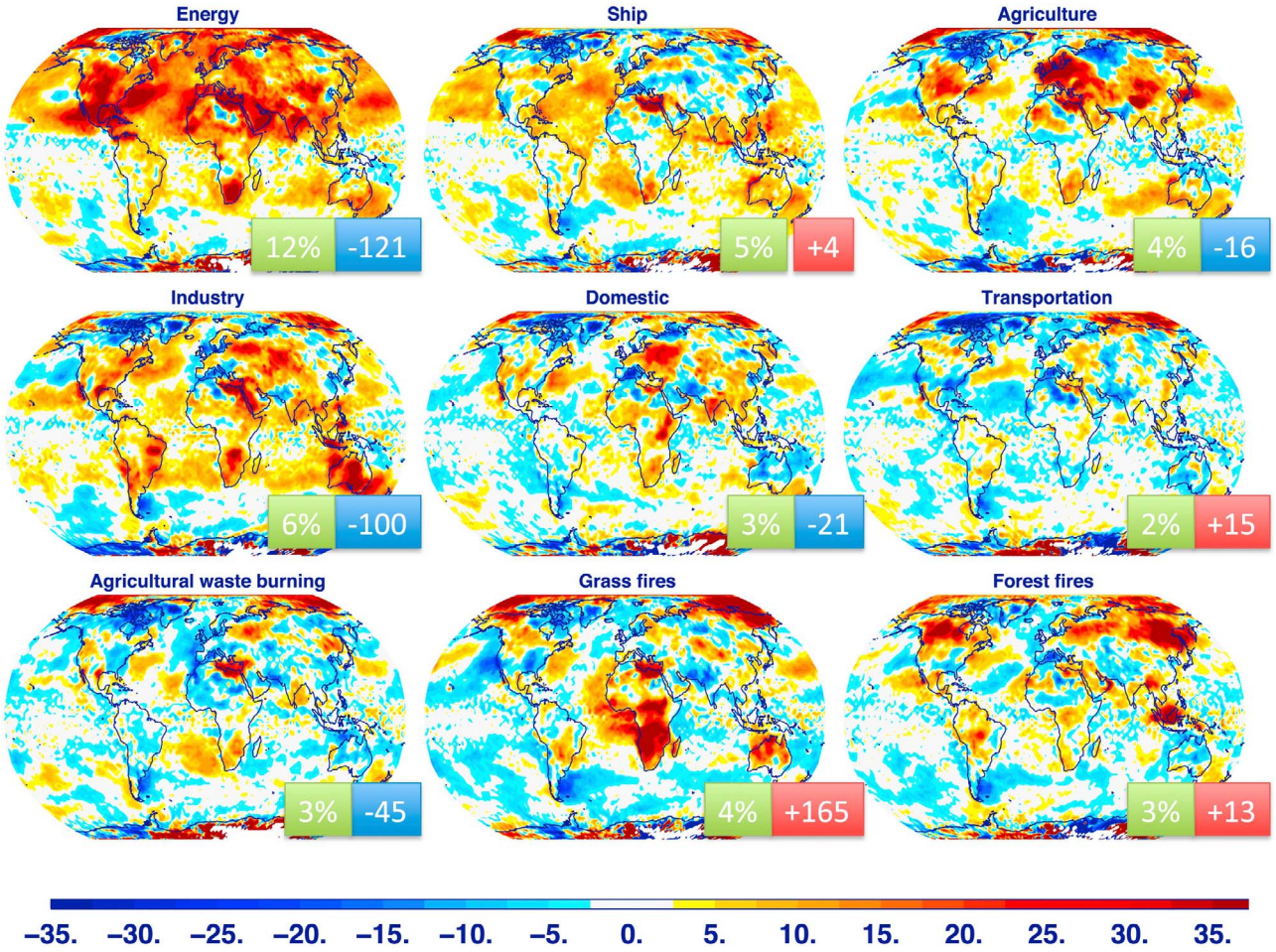

Figure 8. Differences in CDNC (%) per emission sector between a base run and a sector experiment. The base run includes all emission sectors the sector run excludes one sector. The green box gives the global-mean CDNC (%) change and the blue and red boxes give global-mean forcing numbers for Fi (mW/m^2).

forcings Fi and Fs show large variability. In addition, Fs and Fi are often opposite in sign, and it is interesting to note that over the United States all sectors lead to a negative Fi and a positive Fs, whereas in Europe Fs have negative forcings, and most Fi, except for the energy and agricultural (fertilizer) sector that is positive. We speculate that the opposite sign of Fi and Fs must be related to the opposite cloud optical thickness changes as caused by Fs and Fi and discussed in section 3. However, when examining the single regions in more detail, we often see a contrast between east and west within one region. For example, within Europe, pollution toward the west is interacting with maritime air masses leading to lower surface temperatures, and toward more central Europe we notice dryer air and fewer clouds. Eastern Europe, which is exposed to continental air, shows warmer temperatures and increased cloudiness. The few discussed examples demonstrate that we can see expected cloud changes as triggered by semidirect and indirect effects but that even on the regional scale we find cloud changes of similar magnitude but of opposite sign that are indirectly caused by the introduced disturbance, such as CDNC or absorption change. These cloud feedbacks are sometimes dominant over the expected cloud response.

[36] In summary, radiative forcing contributions by process and sector are rather small on the global scale, below ± 0.05 W/m^2, but regionally they have more significant contributions, up to $\pm 1 W/m^2$. The transportation and agricultural waste burning (AWB) sectors are the only sectors that result in a net positive Ft on a global scale. In the United States the transportation sector is the only anthropogenic sector that results in a positive total forcing, whereas in Europe the transportation and AWB have positive forcing numbers. In Asia, domestic emissions have the strongest positive Ft, followed by emissions from industry, transportation, and AWB sector. The chemical composition of domestic emissions in Asia is very different from domestic emissions in Europe and the United States. Asian domestic emissions have a higher proportion of carbonaceous particles, whereas in Europe and the United States the SO_2 fraction is higher.

[37] From a global perspective, transportation and agricultural waste burning are the only overall warming sectors and can be attractive targets for mitigation. However, regionally the following mitigation sectors could be tackled: transportation in the United States, agricultural practices and transportation in Europe, and domestic emissions followed

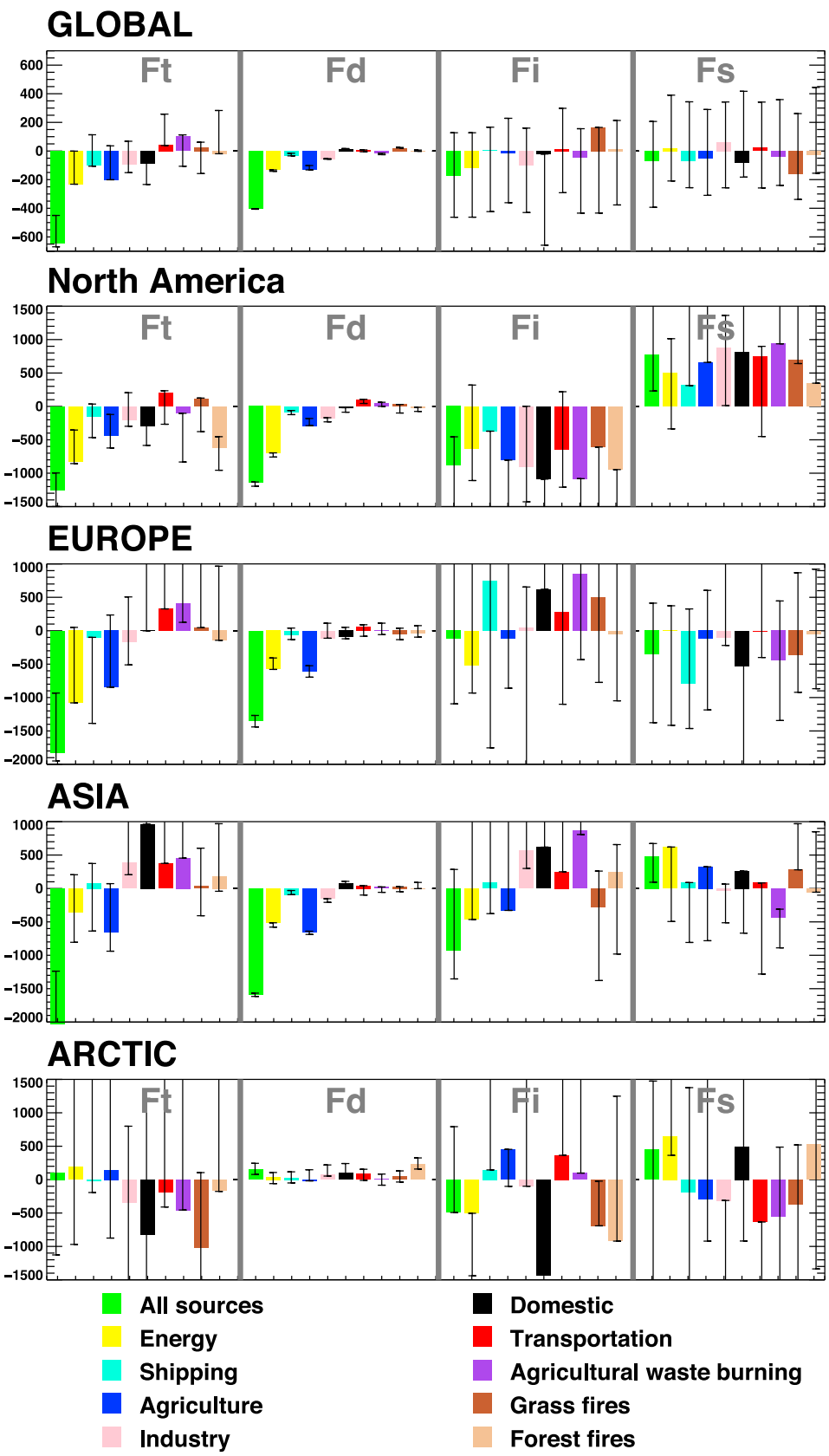

Figure 9. Net (Ft), direct (Fd), indirect (Fi), and semidirect (Fs) radiative forcing changes (mW/m^2) by sector and region. Error bars indicated uncertainty based on annual variability. Regions are United States (129°E–64°E, 21.°N–55.°N), Europe (11°E–46°W, 35.°N–71.°N), Asia (71°W–131°W, 7°N–47°N) and the Arctic (70°N–90°N)

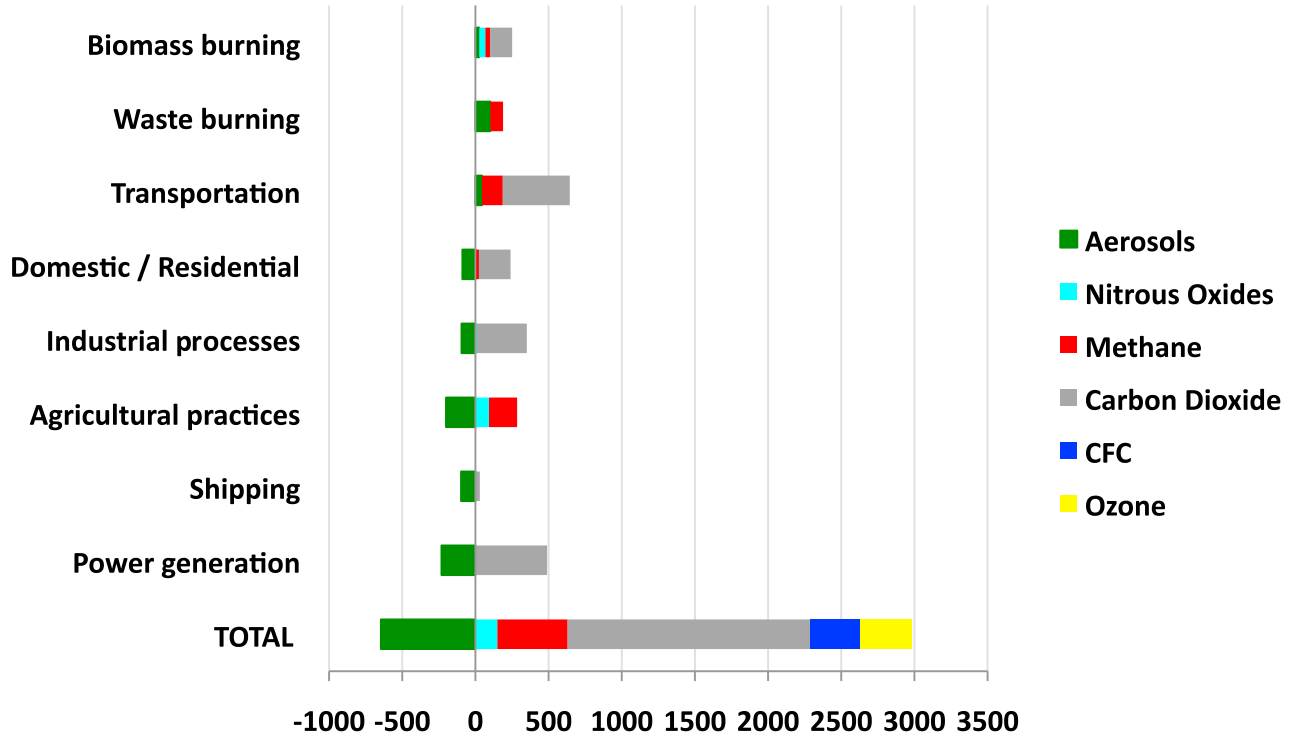

Figure 10. Radiative forcing (mW/m^2) by economic sector. Aerosol forcing numbers are taken from this study N_2O, CH_4, CO_2, CFC, and ozone forcing numbers are taken from the IPPC AR4 report and the EDGAR v32 (http://edgar.jrc.ec.europa.eu) emission inventory.

by agricultural waste burning, industry, and transportation in Asia.

5. Discussion and Conclusions

[38] In this study we tested the emission inventory that is currently used in climate models for the Climate Model Intercomparison Program 5 (CMIP5) in support of the Intergovernmental Panel on Climate Change (IPCC) Fifth Assessment report (AR5). Aerosol forcings, separated into direct, indirect, semidirect, and surface absorptions, were tested for the CMIP5 emission sectors with a climate model that includes detailed aerosol microphysics.

[39] Within the past 150 years net radiative forcing increased by 1.8 W/m^2 caused by increased greenhouse gases and changed atmospheric gas and aerosol concentrations. Aerosol forcing accounts for −0.6 W/m^2 and is masking a substantial portion of the GHG-induced climate change. The largest contribution of the total aerosol forcing is attributed to the direct effect. Here it is interesting to note that aerosol extinction increases everywhere in the polluted regions, but aerosol absorption, which is mostly related to BC concentration changes and its internal mixing state, decreases over the United States but strongly increases over China. This is related to the large preindustrial carbonaceous emission fluxes in the CMIP5 emission data sets and was not present in previous simulations. The second largest negative forcing after the direct forcing is from aerosol indirect effect (the first aerosol indirect effect). Here as well mixing state effects involving carbonaceous aerosols influence the cloud droplet number concentrations, resulting in strongest impacts over Europe and China. Semidirect effects, which eventually can either lead to cloud increase or decrease depending on aerosol type, location, and meteorological conditions, show large spatial variability and therefore on the global-scale cloud changes cancel each other. The resulting forcing is still negative because in our model, surface forcing effects, which induce changes in boundary layer dynamics and cloud feedbacks, dominate over absorption effects on clouds that more likely would promote cloud reduction. Surface albedo effects have a small positive forcing, but cloud feedbacks triggered by this forcing can lead to a 10 times larger radiative flux change at the top of the atmosphere.

[40] Sector studies can provide important information to policy makers, as it is more closely linked to emission regulations than understanding the impact on climate forcing of a particular chemical component. Our model shows that the contribution by sector varies greatly among different countries. Viewing sector studies as a chance to minimize positive forcing contributions through aerosol processes puts worldwide the transportation sector into focus, accompanied by agricultural burning practices in Europe and Asia and domestic emissions in Asia. Regionally, such individual forcing impulses can have a magnitude of +1 W/m^2 (domestic emissions in Asia), though global aerosol forcing numbers remain small compared to other forcing agents. Figure 10 puts the total aerosol forcing numbers by economical sector from this study into perspective with GHG and ozone forcing (these values are taken from *IPCC* [2007]). This comparison clearly illustrates that reducing emissions from sectors with small positive aerosol forcings, e.g., transportation emissions, would lead to a greater benefit due to the large amount of GHG that are emitted from those

sources. However, even sectors leading to negative aerosol forcings, such as power generation, would possibly have a positive net effect on climate due to the effect of coemitted GHG. However, it should be taken into account that competing effects between short-lived species, such as aerosols, and long-lived GHG act on very different time scales.

[41] This study, performed with fixed SSTs, does not account for ocean heat transport. Surface air temperature changes are only simulated over land, although sensible and latent heat fluxes are simulated over all surfaces. The next step would be to study aerosol–cloud interactions including an interactive ocean and ice sheets. *Wang* [2004] found much larger cloud changes when using a Q flux model compared to a model with fixed SSTs. *Allen and Sherwood* [2010, 2011], on the other hand, found that the impact of anthropogenic aerosols in a climate model is more pronounced with fixed SST simulations rather than using a Q flux ocean, apparently because the contrast in land-ocean heating drives a wave number 2 response in the Northern Hemisphere which is more efficient in reaching the stratosphere, showing that zonal heating variations also affect this particular response.

[42] A further limitation of this study is that gas-phase ozone-NO_x-HNO_3 chemistry was decoupled in the simulation, possibly causing biases in the nitrate cycle in the nitrogen-rich sector experiments, such as agriculture.

Appendix A: Model Description

[43] The Goddard Institute for Space Studies (GISS) General Circulation Model (GCM) climate modelE [*Hansen et al.*, 2005; *Schmidt et al.*, 2006] coupled to the aerosol microphysics and chemistry model MATRIX (Multiconfiguration Aerosol Tracker of mixing state) [*Bauer et al.*, 2008] is used in this study. MATRIX is designed to support model calculations of the direct and indirect effect and to permit detailed treatment of aerosol mixing state, size, and aerosol-cloud activation.

[44] MATRIX is based on the quadrature methods of moments (QMOM) including two moments, number and mass, and one quadrature point. Carrying only two moments requires additional information about the shapes of the individual aerosol size distributions. We assume a lognormal distribution with constant width when calculating the initial size distributions, the conversion between aerosol mass and number concentration, emission distributions, coagulation rates, and aerosol optical properties.

[45] For each aerosol population, defined by mixing state and size distribution, the tracked species are number concentration and mass concentration of sulfate, nitrate, ammonium, aerosol water, black carbon, organic carbon, mineral dust, and sea salt. Here we use the aerosol population setup called "mechanism 1" [see *Bauer et al.*, 2008, Table 1]. MATRIX dynamics includes nucleation, new particle formation, particle emissions, gas-particle mass transfer, aerosol phase chemistry, condensational growth, coagulation, and cloud activation.

[46] To simulate the indirect effect, we follow a treatment similar to that described by *Menon et al.* [2010] that includes several changes to the treatment of cloud drop and ice crystal nucleation following the scheme from *Morrison and Gettelman* [2008]. For cloud droplets, we use a prognostic equation to calculate CDNC, based on the work by *Morrison and Gettelman* [2008]. The source term is obtained from MATRIX using the scheme of *Abdul-Razzak and Ghan* [2000] that is based on the Köhler theory for multiple external lognormal modes that are composed of internally mixed soluble and insoluble material.

[47] The model calculates BC deposition on ice and snow surfaces and its impact on albedo as described by *Koch and Hansen* [2005]. To represent BC deposition on snow/ice surfaces and modifications to snow/ice albedo, BC concentrations in the top layer of snow (land and sea ice) are used to calculate the albedo reduction on snow grains with sizes varying from 0.1 to 1 mm [*Koch et al.*, 2009].

[48] In this paper we use the updated version of GISS modelE. The GISS modelE contributions to the CMIP5 archive are improved over the configurations used in CMIP3 (and described by *Schmidt et al.* [2006] and *Hansen et al.* [2007]) in a number of respects. First, the model grid has a higher horizontal and vertical resolution (2° latitude × 2.5° longitude, 40 layers). Second, various physics components have been upgraded from the CMIP3 version, namely, the convection scheme, stratiform cloud scheme, gravity wave drag, sea ice, and ocean physics.

[49] The convection and cloud changes can be summarized as follows: (1) Convective entrainment and updraft speed are diagnosed using the parameterization of *Gregory* [2001], as described by *Del Genio et al.* [2007]. (2) Convective condensate in small particles whose fall speeds are significantly less than the updraft speed is transported upward rather than immediately detraining as by *Del Genio et al.* [2005]; the portion of frozen condensate in the form of graupel extends up to a minimum temperature that depends on updraft speed. (3) Downdrafts originate from multiple levels above cloud base and detrain at all lower levels including below cloud base; downdrafts entrain/detrain momentum as well as heat and moisture; downdraft mass fluxes are used to calculate a gustiness correction to surface fluxes. (4) The convective pressure gradient is assumed to reduce convective momentum transport as by *Gregory et al.* [1997]. (5) The adjustment time for convection to adjust the cloud base to neutral buoyancy is set to 1 h, twice the physics time step.

[50] The model also includes changes to the stratiform cloud parameterization, among them the following: (1) The threshold relative humidity for cloud formation is a function of the large-scale vertical velocity above the boundary layer, with a scale-aware correction for layer thickness; within the boundary layer the threshold relative humidity is based on an assumed Gaussian distribution of saturation deficit as by *Siebesma et al.* [2003]; stratiform clouds do not form in subsaturated air below cloud top in the convective portion of the grid box or below the cloud base of a boundary layer convective cloud. (2) The phase in which cloud forms is maintained until the cloud dissipates unless supercooled liquid is glaciated by the Bergeron-Findeisen process; convective snow is no longer permitted to glaciate a supercooled stratiform cloud. (3) The critical supersaturation for homogeneous nucleation of ice is based on the results of *Kärcher and Lohmann* [2002]. (4) The optical thickness of precipitation is accounted for by the radiation. (5) In unfavorable conditions, stratiform cloud erosion by evaporation up to the threshold relative humidity is allowed. (6) Various changes

to the values of parameters that affect autoconversion, maximum cloud particle size, and the temperature dependence of liquid versus ice formation have been made.

[51] **Acknowledgments.** This work has been supported by the NASA MAP program Modeling, Analysis and Prediction Climate Variability and Change (NN-H-04-Z-YS-008-N) and (NN-H-08-Z-DA-001-N). S.M. was also supported by the U.S. Department of Energy under contract DE-AC02-05CH11231 at LBNL and the DOE Earth System Modeling Program. We thank Greg Faluvegi for processing the emission data sets for the GISS model.

References

Abdul-Razzak, H., and S. J. Ghan (2000), A parameterization of aerosol activation: 2. Multiple aerosol types, *J. Geophys. Res.*, *105*, 6837–6844, doi:10.1029/1999JD901161.

Allen, R. J., and S. C. Sherwood (2010), Aerosol-cloud semi-direct effect and land-sea temperature contrast in a GCM, *Geophys. Res. Lett.*, *37*, L07702, doi:10.1029/2010GL042759.

Allen, R. J., and S. C. Sherwood (2011), The impact of natural versus anthropogenic aerosols on atmospheric circulation in the Community Atmosphere Model, *Clim. Dyn.*, *36*, 1959–1978, doi:10.1007/s00382-010-0898-8.

Bauer, S. E., D. Wright, D. Koch, E. Lewis, R. McGraw, L.-S. Chang, S. Schwarz, and R. Ruedy (2008), Matrix (multiconfiguration aerosol tracker of mixing state): An aerosol microphysical module for global atmospheric models, *Atmos. Chem. Phys.*, *8*, 6003–6035, doi:10.5194/acp-8-6003-2008.

Bauer, S. E., S. Menon, D. Koch, T. C. Bond, and K. Tsigaridis (2010), A global modeling study on carbonaceous aerosol microphysical characteristics and radiative forcing, *Atmos. Chem. Phys.*, *10*, 7439–7456, doi:10.5194/acp-10-7439-2010.

Bond, T., D. Streets, K. Yarber, S. Nelson, J.-H. Wo, and Z. Klimont (2004), A technology-based global inventory of black and organic carbon emissions from combustion, *J. Geophys. Res.*, *109*, D14203, doi:10.1029/2003JD003697.

Chen, W.-T., Y. H. Lee, P. J. Adams, A. Nenes, and J. H. Seinfeld (2010), Will black carbon mitigation dampen aerosol indirect forcing?, *Geophys. Res. Lett.*, *37*, L09801, doi:10.1029/2010GL042886.

Clarke, A. D., and K. J. Noone (1985), Soot in the Arctic snowpack—A cause for perturbations in radiative-transfer, *Atmos. Environ.*, *19*(12), 2045–2053, doi:10.1016/0004-6981(85)90113-1.

Del Genio, A. D., W. Kovari, M.-S. Yao, and J. Jonas (2005), Cumulus microphysics and climate sensitivity, *J. Clim.*, *18*, 2376–2387, doi:10.1175/JCLI3413.1.

Del Genio, A. D., M.-S. Yao, and J. Jonas (2007), Will moist convection be stronger in a warmer climate?, *Geophys. Res. Lett.*, *34*, L16703, doi:10.1029/2007GL030525.

Flanner, M. G., C. S. Zender, J. T. Randerson, and P. J. Rasch (2007), Present-day climate forcing and response from black carbon in snow, *J. Geophys. Res.*, *112*, D11202, doi:10.1029/2006JD008003.

Flanner, M. G., C. S. Zender, P. G. Hess, N. M. Mahowald, T. H. Painter, V. Ramanathan, and P. J. Rasch (2009), Springtime warming and reduced snow cover from carbonaceous particles, *Atmos. Chem. Phys.*, *9*, 2481–2497, doi:10.5194/acp-9-2481-2009.

Gregory, D. (2001), Estimation of entrainment rate in simple models of convective clouds, *Q. J. R. Meteorol. Soc.*, *127*, 53–72, doi:10.1002/qj.49712757104.

Gregory, D., R. Kershaw, and P. Inness (1997), Parametrization of momentum transport by convection. II: Tests in single column and general circulation models, *Q. J. R. Meteorol. Soc.*, *123*, 1153–1183, doi:10.1002/qj.49712354103.

Hansen, J., and L. Nazarenko (2004), Soot climate forcing via snow and ice albedos, *Proc. Natl. Acad. Sci. U. S. A.*, *101*, 423–428, doi:10.1073/pnas.2237157100.

Hansen, J., et al. (2005), Efficacy of climate forcings, *J. Geophys. Res.*, *110*, D18104, doi:10.1029/2005JD005776.

Hansen, J., et al. (2007), Climate simulations for 1880–2003 with GISS modelE, *Clim. Dyn.*, *29*, 661–696, doi:10.1007/s00382-007-0255-8.

Intergovernmental Panel on Climate Change (IPCC) (2001), *Climate Change: The Scientific Basis*, edited by J. T. Houghton et al., 881 pp., Cambridge Univ. Press, Cambridge, U. K.

Intergovernmental Panel on Climate Change (IPCC) (2007), *Climate Change: The Physical Science Basis*, edited by S. Solomon et al., 996 pp., Cambridge Univ. Press, Cambridge, U. K.

Jacobson, M. Z. (2004), Climate response of fossil fuel and biofuel soot, accounting for soot's feedback to snow and sea ice albedo and emissivity, *J. Geophys. Res.*, *109*, D21201, doi:10.1029/2004JD004945.

Jacobson, M. Z. (2010), Short-term effects of controlling fossil-fuel soot, biofuel soot and gases, and methane on climate, Arctic ice, and air pollution health, *J. Geophys. Res.*, *115*, D14209, doi:10.1029/2009JD013795.

Kärcher, B., and U. Lohmann (2002), A parameterization of cirrus cloud formation: Homogeneous freezing of supercooled aerosols, *J. Geophys. Res.*, *107*(D2), 4010, doi:10.1029/2001JD000470.

Koch, D., and A. D. Del Genio (2010), Black carbon absorption effects on cloud cover: Review and synthesis, *Atmos. Chem. Phys.*, *10*, 7685–7696, doi:10.5194/acp-10-7685-2010.

Koch, D., and J. Hansen (2005), Distant origins of Arctic black carbon: A Goddard Institute for Space Studies ModelE experiment, *J. Geophys. Res.*, *110*, D04204, doi:10.1029/2004JD005296.

Koch, D., T. C. Bond, D. Streets, N. Unger, and G. van der Werf (2007), Global impacts of aerosols from particular source regions and sectors, *J. Geophys. Res.*, *112*, D02205, doi:10.1029/2005JD007024.

Koch, D., S. Menon, A. Del Genio, S. Warren, R. Ruedy, I. Alienov, and G. Schmidt (2009), Distinguishing aerosol impacts on climate over the past century, *J. Clim.*, *22*, 2659–2677, doi:10.1175/2008JCLI2573.1.

Koch, D., et al. (2011a), Soot microphysical effects on liquid clouds, a multi-model investigation, *Atmos. Chem. Phys.*, *11*, 1051–1064, doi:10.5194/acp-11-1051-2011.

Koch, D., et al. (2011b), Coupled aerosol-chemistry-climate twentieth century transient model investigation: Trends in short-lived species and climate responses, *J. Clim.*, *24*, 2693–2714, doi:10.1175/2011JCLI3582.1.

Lamarque, J.-F., et al. (2010), Historical (1850–2000) gridded anthropogenic and biomass burning emissions of reactive gases and aerosols: Methodology and application, *Atmos. Chem. Phys.*, *10*, 7017–7039, doi:10.5194/acp-10-7017-2010.

Menon, S., D. Koch, G. Beig, S. Sahu, J. Fasullo, and D. Orlikowski (2010), Black carbon aerosols and the third polar ice cap, *Atmos. Chem. Phys.*, *10*, 4559–4571, doi:10.5194/acp-10-4559-2010.

Morrison, H., and A. Gettelman (2008), A new two-moment bulk stratiform cloud microphysics scheme in the Community Atmospheric Model (CAM3), Part I: Description and numerical tests, *J. Clim.*, *21*(15), 3642–3659, doi:10.1175/2008JCLI2105.1.

Randles, C. A., and V. Ramaswamy (2010), Direct and semi-direct impacts of absorbing biomass burning aerosol on the climate of southern Africa: A Geophysical Fluid Dynamics Laboratory GCM sensitivity study, *Atmos. Chem. Phys.*, *10*(20), 9819–9831, doi:10.5194/acp-10-9819-2010.

Schmidt, G. A., et al. (2006), Present day atmospheric simulations using GISS modelE: Comparison to in-situ, satellite and reanalysis data, *J. Clim.*, *19*, 153–192, doi:10.1175/JCLI3612.1.

Siebesma, A. P., C. S. Bretherton, A. Brown, A. Chlond, J. Cuxart, P. G. Duynkerke, H. Jiang, M. Khairoutdinov, D. Lewellen, and C. H. Moeng (2003), A large eddy simulation intercomparison study of shallow cumulus convection, *J. Atmos. Sci.*, *60*, 1201–1219, doi:10.1175/1520-0469(2003)60<1201:ALESIS>2.0.CO;2.

Unger, N. (2011), Global climate impact of civil aviation for standard and desulfurized jet fuel, *Geophys. Res. Lett.*, *38*, L20803, doi:10.1029/2011GL049289.

Unger, N., D. T. Shindell, D. M. Koch, and D. G. Streets (2008), Air pollution radiative forcing from specific emissions sectors at 2030, *J. Geophys. Res.*, *113*, D02306, doi:10.1029/2007JD008683.

Unger, N., T. C. Bond, J. S. Wang, D. M. Koch, S. Menon, D. T. Shindell, and S. Bauer (2010), Attribution of climate forcing to economic sectors, *Proc. Natl. Acad. Sci. U. S. A.*, *107*, 3382–3387, doi:10.1073/pnas.0906548107.

Wang, C. (2004), A modeling study on the climate impacts of black carbon aerosols, *J. Geophys. Res.*, *109*, D03106, doi:10.1029/2003JD004084.

Wild, M., H. Gilgen, A. Roesch, A. Ohmura, C. N. Long, E. G. Dutton, B. Forgan, A. Kallis, V. Russak, and A. Tsvetkov (2005), From dimming to brightening: Decadal changes in solar radiation at Earth's surface, *Science*, *308*(5723), 847–850, doi:10.1126/science.1103215.

Zelinka, M. D., and D. L. Hartmann (2010), Why is longwave cloud feedback positive?, *J. Geophys. Res.*, *115*, D16117, doi:10.1029/2010JD013817.

S. E. Bauer, NASA Goddard Institute for Space Studies, 2880 Broadway, New York, NY 10025-0000, USA. (sb2273@columbia.edu)

S. Menon, Lawrence Berkeley National Laboratory, 1 Cyclotron Rd., Berkeley, CA 94720, USA.